Available online at www.sciencedirect.com
SCIENCE DIRECT
Journal of Process Control 16 (2006) 733–745
JOURNAL OF PROCESS CONTROL
www.elsevier.com/locate/jprocont

Feedforward control with online parameter estimation applied to the Chylla–Haase reactor benchmark

Knut Graichen [a,*], Veit Hagenmeyer [b], Michael Zeitz [a]

[a] *Institut für Systemdynamik, Universität Stuttgart, Pfaffenwaldring 9, 70569 Stuttgart, Germany*
[b] *BASF Aktiengesellschaft, Engineering Service Center Automation Technology, WLE/ED-L440, 67056 Ludwigshafen, Germany*

Received 22 July 2005; received in revised form 9 January 2006; accepted 15 January 2006

Abstract

The Chylla–Haase polymerization reactor is used as a benchmark problem to illustrate the potential of feedforward control design by extending the conventional cascade control in the framework of the two-degree-of-freedom control concept. To ensure an accurate temperature control, the feedforward control is adapted to different batch conditions and various products by an extended Kalman filter. The reaction heat and the heat transfer coefficient are estimated online based on simple physically motivated relations applicable to a wider range of batch reactors. Simulation results under model uncertainties show the effectiveness and accuracy of the adaptive feedforward control concept while maintaining the conventional feedback cascade control.

Keywords: Two-degree-of-freedom control; Feedforward control; Cascade control; Extended Kalman filter; Online parameter estimation; Batch process operation

1. Introduction

Batch and semi-batch reactors are widely used in chemical industry for the production of fine chemicals, pigments, polymers, and pharmaceuticals. Generally, the processes can be split in a heat-up interval and a subsequent production period with highly nonlinear exothermic reactions requiring an exact temperature control. A respective control engineering benchmark problem is the polymerization reactor described by Chylla and Haase [2,3]. The control task comprises the heat-up of the reactor to the operation temperature before the monomer feed starts, and subsequently keeping the temperature constant throughout the production. Thereby, the step-like monomer feed poses a significant demand on the control in order to keep the reactor temperature within a specified tolerance interval. In the benchmark scenario, the operation of the reactor must be guaranteed for two different products and under various disturbing influences, e.g., changing ambient temperatures in winter and summer, or impurity of the monomer.

Industrial polymerization reactors are usually controlled by a cascade structure consisting of a master controller for the reactor temperature and an underlying slave controller for the cooling circuit. The cascade control provides a robust operation, but often lacks in control performance concerning the required strict temperature tolerances [2]. Therefore, various control concepts have been used in the literature to deal with the benchmark problem. A model predictive controller is used in [7] combined with an extended Kalman filter for the estimation of the reaction heat and heat transfer coefficient. In [8], the control task of keeping the reactor temperature constant during the production is solved as an optimal control problem by minimizing a cost function for the deviation of the reactor temperature from the desired temperature setpoint. A nonlinear adaptive

* Corresponding author. Tel.: +49 711 685 6568; fax: +49 711 685 6371.
E-mail addresses: knut.graichen@isr.uni-stuttgart.de (K. Graichen), veit.hagenmeyer@basf-ag.de (V. Hagenmeyer), michael.zeitz@isys.uni-stuttgart.de (M. Zeitz).

0959-1524/$ - see front matter © 2006 Elsevier Ltd. All rights reserved.
doi:10.1016/j.jprocont.2006.01.001

controller is designed in [4] to adjust the cooling jacket temperature, which serves as the setpoint for an underlying PI controller of the cooling jacket. A further approach [1] deals with the design of a neural network controller to maintain the reactor temperature at its setpoint, whereby the control valve toggles between maximum and minimum position, which is certainly not practicable in industry.

The control concept presented in this contribution solves the Chylla–Haase benchmark problem by extending the conventional cascade control with a feedforward control for the cooling jacket temperature in order to improve the performance of the temperature control. The feedforward control design is based on the inverse reactor model and calculates a feedforward trajectory for the cooling jacket temperature in order to follow a predefined trajectory of the reactor temperature. Thereby, the reaction heat as well as the heat transfer coefficient in the energy balance are estimated online by an extended Kalman filter. Two simple physically motivated relations are employed, which allow the non-delayed and accurate estimation of both quantities.

The paper is organized as follows: the next section describes the Chylla–Haase control problem and the respective reactor model, and explains the conventional cascade control structure. In Section 3, the reactor model is used for the offline calculation of the nominal feedforward control, which illustrates the achievable performance of the cascade control in combination with a feedforward control. In Section 4, the adaptive feedforward control design is described, whereby a simplified reactor model is used for the design of an extended Kalman filter in order to estimate the states as well as the reaction heat and the heat transfer coefficient. These estimates are used for the online adaptation of the feedforward control. Finally, Section 5 provides simulation studies and a robustness analysis for various batches and disturbances illustrating the performance and robustness of the proposed control scheme.

2. The Chylla–Haase benchmark reactor

The industrial polymerization process described by Chylla and Haase [2,3] consists of a stirred tank reactor with a cooling jacket and a coolant recirculation, see Fig. 1. The reactor temperature is controlled by manipulating the temperature of the coolant which is recirculated through the cooling jacket of the reactor. The slave controller can act in two modes: in cooling mode, cold water is inserted into the recirculation loop, whereas in heating mode steam is injected into the recirculating water stream. In [2], data is given for two different products A and B. The recipes for the products comprise two consecutive control tasks:

- Heating up of the reactor to a constant setpoint before the monomer feed $\dot{m}_{\mathrm{M}}^{\mathrm{in}}(t)$ starts.
- Keeping the reactor temperature $T(t)$ within a tolerance interval of ± 0.6 K during the monomer feed and after a subsequent specified hold period.

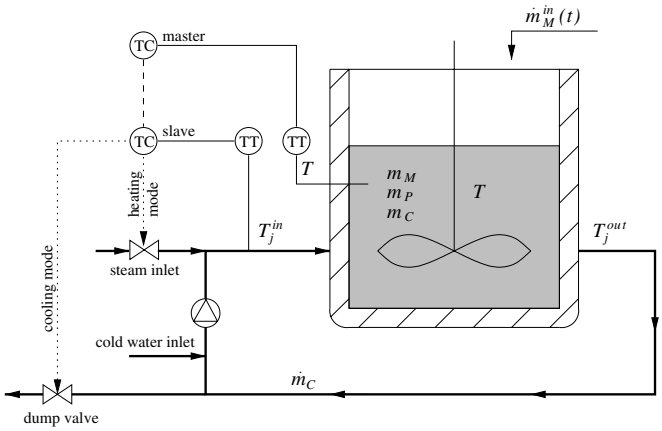

Fig. 1. Reactor schematic with cooling circuit, monomer feed $\dot{m}_{\mathrm{M}}^{\mathrm{in}}(t)$, master and slave controller for the reactor temperature T (TT = temperature transmitter, TC = temperature controller).

Thereby, the monomer feed $\dot{m}_{\mathrm{M}}^{\mathrm{in}}(t)$ starts and ends abruptly at specified time points. The respective polymer A or B is produced in five subsequent batches, and is removed between the batches. However, the reactor is only cleaned after the fifth batch. The control tasks are complicated by several features of the polymerization process [2]:

- The production of the polymers A and B is characterized by different reaction kinetics and heat production.
- The heat transfer coefficient decreases significantly during a batch due to an increasing batch viscosity, and from batch to batch due to surface fouling.
- The reaction kinetics are nonlinear and subject to the gel effect.

2.1. Polymerization reactor model

A dynamic model of the polymerization reactor has been derived by Chylla and Haase [2,3] based on simplified kinetic relations. The temperature dynamics are captured by considering energy balances for the reactor and the cooling jacket. Moreover, the following corrections have been proposed in the literature:

- A corrected energy balance for the reactor temperature is derived in [7].
- The precharge of the reactor consisting of prepolymer and water as given in the original paper [2] exceeds the reactor volume, see [7]. This problem is addressed in [8] by assuming smaller values such that the reactor volume is not exceeded after production (see Table A.2 for the respective data).
- The heat transfer coefficient is limited to a minimum value of $0.2\ \mathrm{kW\,m^{-2}\,K^{-1}}$ [7]. This is necessary because the heat transfer coefficient between wall and reactor falls to zero during the production of polymer B making it impossible to further control the reactor temperature.

The corrected model of the Chylla–Haase reactor is given by

$$\frac{\mathrm{d}m_\mathrm{M}}{\mathrm{d}t} = \dot{m}_\mathrm{M}^\mathrm{in}(t) + \frac{Q_\mathrm{rea}}{\Delta H}, \tag{1}$$

$$\frac{\mathrm{d}m_\mathrm{P}}{\mathrm{d}t} = -\frac{Q_\mathrm{rea}}{\Delta H}, \tag{2}$$

$$\frac{\mathrm{d}T}{\mathrm{d}t} = \frac{1}{\sum_i m_i C_{p,i}}\left[\dot{m}_\mathrm{M}^\mathrm{in}(t) C_{p,\mathrm{M}}(T_\mathrm{amb} - T) - UA(T - T_j) - (UA)_\mathrm{loss}(T - T_\mathrm{amb}) + Q_\mathrm{rea}\right] \quad (i = M, P, W), \tag{3}$$

$$\frac{\mathrm{d}T_j^\mathrm{out}}{\mathrm{d}t} = \frac{1}{m_\mathrm{C} C_{p,\mathrm{C}}}\left[\dot{m}_\mathrm{C} C_{p,\mathrm{C}}(T_j^\mathrm{in}(t-\theta_1) - T_j^\mathrm{out}) + UA(T - T_j)\right], \tag{4}$$

$$\frac{\mathrm{d}T_j^\mathrm{in}}{\mathrm{d}t} = \frac{\mathrm{d}T_\mathrm{out}^j(t-\theta_2)}{\mathrm{d}t} + \frac{T_j^\mathrm{out}(t-\theta_2) - T_j^\mathrm{in}}{\tau_p} + \frac{K_p(c)}{\tau_p}. \tag{5}$$

The reactor model comprises the material balances (1) and (2) for the monomer mass $m_\mathrm{M}(t)$ and the polymer mass $m_\mathrm{P}(t)$, the energy balance (3) with the reactor temperature $T(t)$, as well as the energy balances (4) and (5) of the cooling jacket and the recirculation loop with the outlet and inlet temperatures $T_j^\mathrm{out}(t)$ and $T_j^\mathrm{in}(t)$ of the coolant C. Further variables and the parameters of the reactor model are listed in Table 1. The available measurements of the process are the temperatures of the reactor and cooling circuitry:

$$\boldsymbol{y} = [T, T_j^\mathrm{in}, T_j^\mathrm{out}]^\mathrm{T}. \tag{6}$$

The heating/cooling function $K_p(c)$, as defined in [2,3], is influenced by an equal-percentage valve with valve position $c(t)$ and the following split-range valve characteristic

$$K_p(c) = \begin{cases} 0.8 \cdot 30^{-c/50}(T_\mathrm{inlet} - T_j^\mathrm{in}(t)), & c < 50\%, \\ 0, & c = 50\%, \\ 0.15 \cdot 30^{(c/50-2)}(T_\mathrm{steam} - T_j^\mathrm{in}(t)), & c > 50\%. \end{cases} \tag{7}$$

Table 1
Variables and parameters of the reactor model (1)–(5)

$\dot{m}_\mathrm{M}^\mathrm{in}(t)$	Monomer feed rate [kg/s]
$Q_\mathrm{rea} = -\Delta H \cdot R_p$	Reaction heat [kW]
R_p	Rate of polymerization [kg/s]
$-\Delta H$	Reaction enthalpy [kJ kg^{-1}]
U	Overall heat transfer coefficient [kW m^{-2} K^{-1}]
A	Jacket heat transfer area [m^2]
$(UA)_\mathrm{loss}$	Heat loss coefficient [kW/K]
$C_{p,\mathrm{M}}$, $C_{p,\mathrm{P}}$, $C_{p,\mathrm{C}}$	Specific heat at constant pressure [kJ kg^{-1} K^{-1}]
θ_1, θ_2	Transport delay in jacket and recirculation loop [s]
$T_j = (T_j^\mathrm{in} + T_j^\mathrm{out})/2$	Average cooling jacket temperature [K]
$K_p(c)$	Heating/cooling function [K]
τ_p	Heating/cooling time constant [s]

For $c < 50\%$, ice water with inlet temperature T_inlet is inserted in the cooling jacket, whereas a valve position $c > 50\%$ leads to a heating of the coolant by injecting steam with temperature T_steam into the recirculating water stream.

The time intervals of the monomer feed $\dot{m}_\mathrm{M}^\mathrm{in}(t)$ are specified in the recipes for polymer A and B [2]. For polymer A, a single feed interval $t \in [t_{\mathrm{M},0}^\mathrm{in}, t_{\mathrm{M},1}^\mathrm{in}]$ is considered, whereas the recipe of polymer B additionally comprises a second feed period $t \in [t_{\mathrm{M},2}^\mathrm{in}, t_{\mathrm{M},3}^\mathrm{in}]$ with a specified hold period between the two feeds, i.e.,

$$\dot{m}_\mathrm{M}^\mathrm{in}(t) = \begin{cases} \dot{m}_\mathrm{M}^\mathrm{in,max}, & \text{if } t \in [t_{\mathrm{M},0}^\mathrm{in}, t_{\mathrm{M},1}^\mathrm{in}] \text{ or } t \in [t_{\mathrm{M},2}^\mathrm{in}, t_{\mathrm{M},3}^\mathrm{in}] \text{ (polymer } B), \\ 0, & \text{else.} \end{cases} \tag{8}$$

Table 2 summarizes the empirical relations for R_p, A, and U taken from [2,8]. A detailed description of these relations is given in [2]. The parameter values of the model and the polymers A and B are listed in Tables A.1 and A.2 of Appendix A.

2.2. Uncertainties and disturbances in the process

Various disturbances and uncertainties are specified in [2], in order to model the following practical problems with the control of polymerization reactors:

Table 2
Empirical relations for the polymerization rate R_p, the jacket heat transfer area A, and the overall heat transfer coefficient U [2,8]

$R_p = ikm_\mathrm{M}$ with	i	Impurity factor [–]
	$k = k_0 \exp\left(-\frac{E}{RT}\right) \cdot (k_1\mu)^{k_2}$	First-order kinetic const. [s^{-1}]
	$\mu = c_0 \exp(c_1 f) \cdot 10^{c_2(a_0/T - c_3)}$	Batch viscosity [kg m^{-1} s^{-1}]
	$f = m_\mathrm{P}/(m_\mathrm{M} + m_\mathrm{P} + m_\mathrm{C})$	Auxiliary variable [–]
	k_0, k_1, E, R, a_0, c_0, c_1, c_2, c_3	Constants, see Table A.1
	R	Natural gas const. [kJ kmol^{-1} K^{-1}]
$A = \left(\frac{m_\mathrm{M}}{\rho_\mathrm{M}} + \frac{m_\mathrm{P}}{\rho_\mathrm{P}} + \frac{m_\mathrm{W}}{\rho_\mathrm{W}}\right)\frac{P}{B_1} + B_2$ with	ρ_M, ρ_P, ρ_C	Densities [kg m^{-3}]
	B_1	Reactor bottom area [m]
	P	Jacket perimeter [m]
	B_2	Jacket bottom area [m^2]
$U = \frac{1}{h^{-1} + h_\mathrm{f}^{-1}}$ with	$h = d_0 \exp(d_1 \mu_\mathrm{wall})$	Film heat transfer coefficient [kW m^{-2} K^{-1}]
	$\mu_\mathrm{wall} = c_0 \exp(c_1 f) \cdot 10^{c_2(a_0/T_\mathrm{wall} - c_3)}$	Wall viscosity [kg m^{-1} s^{-1}]
	$T_\mathrm{wall} = (T + T_j)/2$	Wall temperature [K]
	h_f^{-1}	Fouling factor depending on batch no. [m^2 K/kW]
	d_0, d_1	Constants, see Table A.1

- The impurity factor $i \in [0.8, 1.2]$ in the polymerization rate R_p is random and constant during one batch, which tries to model fluctuations in monomer kinetics caused by batch-to-batch variations in reactive impurities [2]. The fouling factor $1/h_f$ in the overall heat transfer coefficient U increases with each batch and accounts for the fact that during successive batches a polymer film builds up on the wall resulting in a decrease of U.
- The delay times θ_1 and θ_2 of the cooling jacket and the recirculation loop may vary by $\pm 25\%$ compared to the nominal values in Table A.2.
- The ambient temperature T_{amb} is different during summer and winter. This effects the temperature of the monomer feed $\dot{m}_{\text{M}}^{\text{in}}(t)$, as well as the initial conditions $T(0)$, $T_j^{\text{in}}(0)$, and $T_j^{\text{out}}(0)$ given by T_{amb}.
- As proposed in [2], measurement noise is added to the temperature measurements (6) with the standard deviation $\sigma(\boldsymbol{y}) = 0.05$ K.

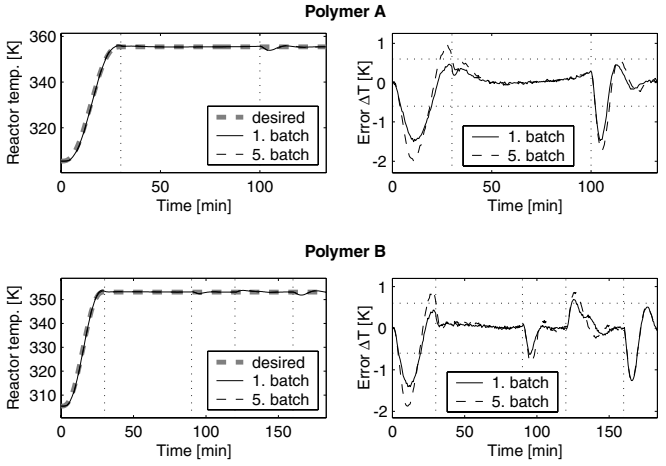

Fig. 2. Reactor temperature $T(t)$ and control error $\Delta T(t)$ of the PI cascade controlled reactor for polymer A and B for nominal parameters and summer season.

2.3. Conventional cascade control structure

A very tight temperature control is necessary in order to produce polymer of a desired quality. The controller should be able to maintain the reactor temperature T within an interval of ± 0.6 K around the desired setpoint under all operation conditions and disturbances [2]. Commonly used for chemical reactors is a PI cascade control structure, which provides a robust operation but often lacks in control performance. The cascade control structure is shown in Fig. 7 as the basis for the proposed adaptive feedforward control concept. The master controller $\Sigma_{\text{FB},1}$ regulates the reactor temperature T by manipulating the setpoint T_j^{set} of the mean cooling jacket temperature T_j. The slave controller $\Sigma_{\text{FB},2}$ adjusts the valve position c in order to control the mean jacket temperature T_j set by the master controller.[1]

In order to heat-up the reactor to the specified setpoint T^{set} before the monomer feed $\dot{m}_{\text{M}}^{\text{in}}(t)$ starts, a trajectory is planned for the desired reactor temperature $T^*(t)$ by the polynomial set-up[2]

$$T^*(t) = \begin{cases} T_{\text{amb}} + (T^{\text{set}} - T_{\text{amb}}) \sum_{i=3}^{5} a_i \left(\frac{t}{t^{\text{heat}}}\right)^i, & \text{if } t \leqslant t^{\text{heat}}, \\ T^{\text{set}}, & \text{if } t > t^{\text{heat}} \end{cases} \tag{9}$$

with $a_3 = 10$, $a_4 = -15$, and $a_5 = 6$. In the first interval $t \leqslant t^{\text{heat}}$, the reactor is heated up to the setpoint T^{set}. For $t > t^{\text{heat}}$, the temperature $T^*(t)$ is kept constant at T^{set}. In the following, the heat-up time is set to $t^{\text{heat}} = 30$ min corresponding to the time instant when the monomer feed $\dot{m}_{\text{M}}^{\text{in}}(t)$ starts.

The simulation results of the reactor with the PI cascade control[3] for polymer A and B are shown in Fig. 2 for the batches 1 and 5. A tracking error ΔT occurs during the heat-up interval, since the reactor temperature $T(t)$ follows the desired trajectory $T^*(t)$ only time-delayed. During the production, the reactor temperature $T(t)$ violates the tolerance interval ± 0.6 K especially at the end of the monomer feed. The temperature error $\Delta T(t)$ is larger during batch no. 5, since the heat transfer coefficient $U(t)$ decreases significantly during the successive batches, see Figs. 8 and 9 in Section 4.1.

3. Feedforward control based on offline calculation

The performance of the cascade control can be significantly improved by an additional feedforward control Σ_{FF} in the spirit of the two-degree-of-freedom control structure, see Fig. 7. The feedforward control Σ_{FF} calculates the feedforward trajectory $T_j^*(t)$ for the mean jacket temperature as the nominal setpoint for the slave controller $\Sigma_{\text{FB},2}$. The master controller $\Sigma_{\text{FB},1}$ stabilizes the reactor temperature along the desired trajectory $T^*(t)$, such that the overall setpoint for the jacket temperature becomes

$$T_j^{\text{set}}(t) = T_j^*(t) + \Delta T_j(t). \tag{10}$$

This section describes the feedforward control design, which is based on the reactor model (1)–(5) and the desired

[1] Commonly, the jacket inlet temperature T_j^{in} is used as manipulated variable for the control of the reactor temperature. In this paper, $T_j = (T_j^{\text{in}} + T_j^{\text{out}})/2$ is used (see Table 1), since T_j—instead of T_j^{in}—appears explicitly in the energy balance (3) of the reactor model.

[2] The polynomial describes a twice differentiable trajectory $T^*(t) \in \mathscr{C}^2$ with $\dot{T}(0) = \ddot{T}(0) = 0$ and $\dot{T}(t^{\text{heat}}) = \ddot{T}(t^{\text{heat}}) = 0$, which the cascade control is more likely to follow than, e.g., a ramp function.

[3] The parameters of the PI control cascade are tuned in simulation studies to $K_{\text{P}}^m = 4$, $T_I^m = 20$ s for the master controller, and $K_{\text{P}}^s = 20$, $T_I^s = 40$ s for the slave controller. These values are also used as controller parameters in the following sections. The sampling time for the slave and the master controller has been set to 4 s. A smaller sampling time for the slave controller or both controllers has shown no nameable performance improvements.

output trajectory $T^*(t)$ in (9). The nominal feedforward control $T_j^*(t)$ illustrates the achievable control performance in combination with the cascade feedback control.

3.1. Inversion-based feedforward control design

The feedforward control design is based on the input–output representation of the reactor model [6]. The energy balance (3) for the output T forms the input–output dynamics [9] of the reactor model and can be abbreviated as

$$\dot{T} = \alpha(\dot{m}_{\mathrm{M}}^{\mathrm{in}}(t), m_{\mathrm{M}}, m_{\mathrm{P}}, T, T_j) \tag{11}$$

in dependence of the states $m_{\mathrm{M}}(t)$, $m_{\mathrm{P}}(t)$, $T(t)$, and the input $T_j(t)$. Note that the feed rate $\dot{m}_{\mathrm{M}}^{\mathrm{in}}(t)$ occurs as a time-varying parameter specified by (8). If the inverse of the input–output dynamics (11) exists, i.e., $\partial\alpha/\partial T_j \neq 0$, the feedforward control

$$T_j^* = \alpha^{-1}(\dot{m}_{\mathrm{M}}^{\mathrm{in}}(t), m_{\mathrm{M}}^*, m_{\mathrm{P}}^*, T^*, \dot{T}^*) \tag{12}$$

can be calculated with respect to a desired output trajectory $T^*(t)$.[4] Additionally, the desired trajectories $m_{\mathrm{M}}^*(t)$ and $m_{\mathrm{P}}^*(t)$ of the monomer and the polymer are required in order to calculate (12). The material balances (1) and (2) form the internal dynamics [9] of the system and are abbreviated by

$$\begin{aligned} \dot{m}_{\mathrm{M}}^* &= \beta_{\mathrm{M}}(\dot{m}_{\mathrm{M}}^{\mathrm{in}}(t), m_{\mathrm{M}}^*, m_{\mathrm{P}}^*, T^*), \quad & m_{\mathrm{M}}^*(0) &= m_{\mathrm{M},0}, \\ \dot{m}_{\mathrm{P}}^* &= \beta_{\mathrm{P}}(\dot{m}_{\mathrm{M}}^{\mathrm{in}}(t), m_{\mathrm{M}}^*, m_{\mathrm{P}}^*, T^*), \quad & m_{\mathrm{P}}^*(0) &= m_{\mathrm{P},0}. \end{aligned} \tag{13}$$

The numerical integration of the internal dynamics that depends on the desired output trajectory $T^*(t)$ corresponds to the stable inversion technique [6] and yields the desired trajectories $m_{\mathrm{M}}^*(t)$ and $m_{\mathrm{P}}^*(t)$.

The nominal feedforward control $T_j^*(t)$ is obtained by placing the trajectories $T^*(t)$, $m_{\mathrm{P}}^*(t)$, and $m_{\mathrm{M}}^*(t)$ into (12). However, Eq. (11) cannot be solved analytically for T_j^*, since the heat transfer coefficient U in the energy balance (3) also depends on the input $T_j^*(t)$. By writing (11) in the residual form

$$\dot{T}^*(t) - \alpha(\dot{m}_{\mathrm{M}}^{\mathrm{in}}(t), m_{\mathrm{M}}^*(t), m_{\mathrm{P}}^*(t), T^*(t), T_j^*(t)) = 0, \tag{14}$$

the feedforward control $T_j^*(t)$ can be determined by numerically solving (14) in each time step $t = t_k$.[5] The resulting trajectories for polymer A and B are shown in Figs. 3 and 4 for the batch no. 1, 3, and 5, respectively. The successive batches require stronger heating or cooling of the cooling jacket due to the decreasing heat transfer coefficient U, which is modeled by the empirical fouling factor h_{f}^{-1} in Table 2. On the other hand, the trajectories

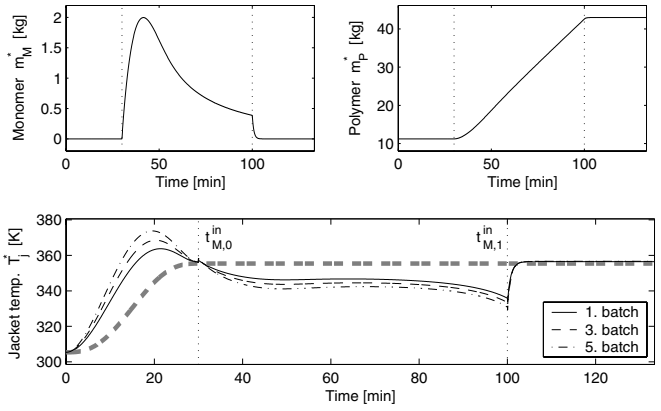

Fig. 3. Design results for polymer A: trajectories $m_{\mathrm{M}}^*(t)$, $m_{\mathrm{P}}^*(t)$, and nominal feedforward control $T_j^*(t)$ together with the desired reactor temperature $T^*(t)$ based on the reference model (1)–(3) for nominal parameters and summer season.

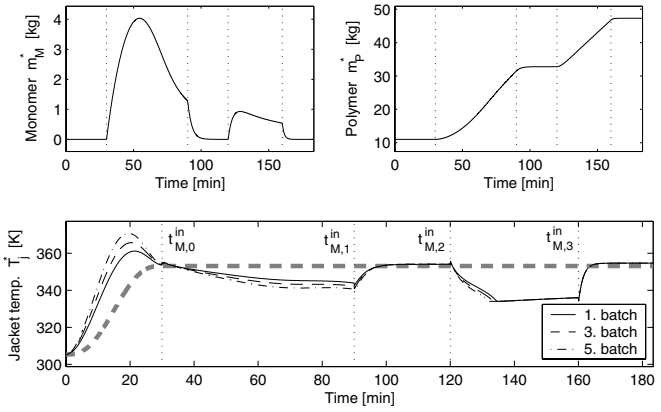

Fig. 4. Design results for polymer B: trajectories $m_{\mathrm{M}}^*(t)$, $m_{\mathrm{P}}^*(t)$, and nominal feedforward control $T_j^*(t)$ together with the desired reactor temperature $T^*(t)$ based on the reference model (1)–(3) for nominal parameters and summer season.

$m_{\mathrm{M}}^*(t)$ and $m_{\mathrm{P}}^*(t)$ for the monomer and the polymer are the same for the different batches, because the reactor temperature $T^*(t)$ is kept constant throughout all batches.

The small overshoot in the feedforward control $T_j^*(t)$ at time instant $t_{\mathrm{M},0}^{\mathrm{in}} = 30$ min (see Table A.1), i.e., when the feed period (8) starts, occurs because the monomer feed $\dot{m}_{\mathrm{M}}^{\mathrm{in}}(t)$ has ambient temperature T_{amb}, whereas the reactor is already heated to the operating temperature T^{set}, see Figs. 3 and 4. Therefore, the reactor is initially cooled by the monomer feed $\dot{m}_{\mathrm{M}}^{\mathrm{in}}(t)$ before the reaction starts. This effect is counteracted by the jacket temperature T_j. Vice versa, a small undershoot in $T_j^*(t)$ occurs at the end of the feed period $t_{\mathrm{M},1}^{\mathrm{in}} = 100$ min ($t_{\mathrm{M},1}^{\mathrm{in}} = 90$ min and $t_{\mathrm{M},3}^{\mathrm{in}} = 160$ min for polymer B) when the monomer feed stops. The feedforward control $T_j^*(t)$ compensates the lack of additional cooling of the monomer feed, before the exothermic reaction ends. In comparison to [8], the inversion-based feedforward control design yields the same feedforward trajectory $T_j^*(t)$ without solving an optimal control problem.

[4] The desired trajectory $T^*(t)$ has to be at least $\mathscr{C}^1$-continuous in order to guarantee $\mathscr{C}^0$-continuity for the feedforward control $T_j^*(t)$. As mentioned before, the desired trajectory $T^*(t)$ in (9) is $\mathscr{C}^2$-continuous and yields a smoother feedforward control $T_j^*(t)$, which is easier to follow by the slave controller.

[5] Thereby must be assumed that (14) can be numerically solved for $T_j^*(t)$ at least locally, i.e., $\partial\alpha/\partial T_j \neq 0$.

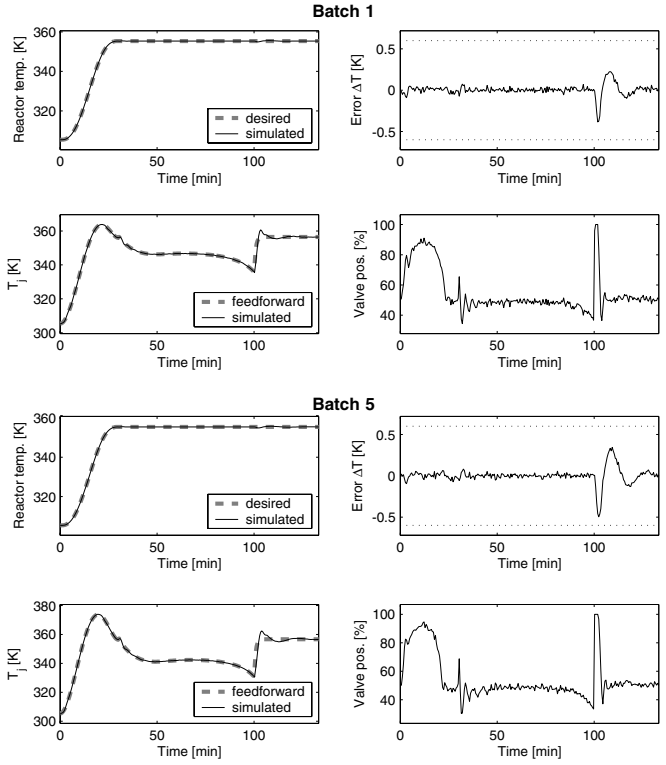

Fig. 5. Simulation results for polymer A: batch no. 1 and 5 with PI cascade control and nominal feedforward control $T_j^*(t)$ for nominal parameters and summer season.

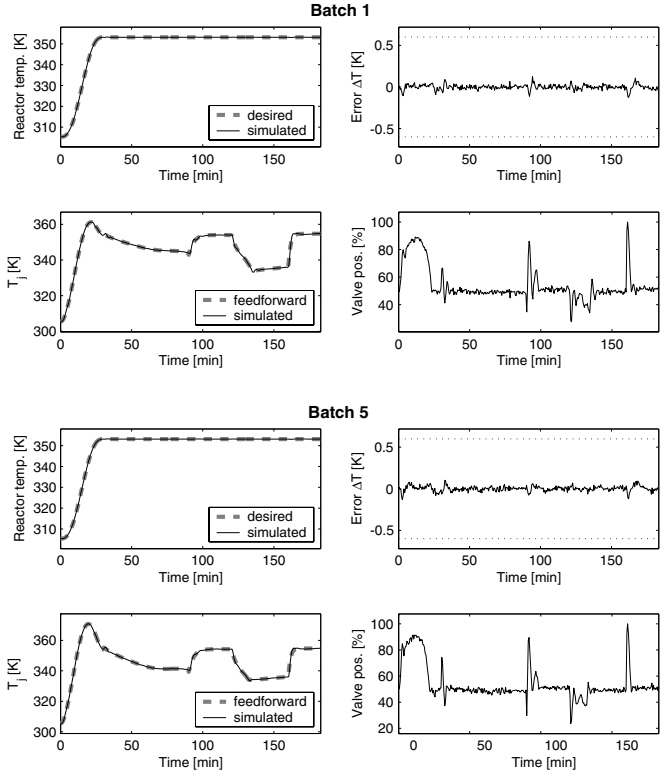

Fig. 6. Simulation results for polymer B: batch no. 1 and 5 with PI cascade control and nominal feedforward control $T_j^*(t)$ for nominal parameters and summer season.

3.2. Simulation results

In order to illustrate the achievable performance, the reactor is simulated with the PI cascade control together with the nominal feedforward control $T_j^*(t)$ calculated from (14). The sampling time of the feedforward control is set to 4 s, which equals the sampling times of the cascade control. The results for polymer A and B in Figs. 5 and 6 show the good performance which the feedforward control achieves in the nominal case. The deviations of the reactor temperature $T(t)$ from $T^*(t)$ are caused by the time-delayed response of the slave controller $\Sigma_{\mathrm{FB},2}$ to the respective set-point $T_j^{\mathrm{set}}(t)$ in (10) adjusted by the master controller $\Sigma_{\mathrm{FB},1}$.

The simulations of the cascade controlled reactor together with the nominal feedforward control $T_j^*(t)$ illustrate that the temperature error $\Delta T(t)$ can be reduced significantly compared to the conventional cascade control without feedforward part, see Fig. 2. The temperature error $\Delta T(t)$ stays within the tolerance interval ± 0.6 K during the heat-up, as well as for the critical time points when the monomer feed $\dot{m}_{\mathrm{M}}^{\mathrm{in}}(t)$ starts and stops.

4. Adaptive feedforward control scheme

The inversion-based calculation of the nominal feedforward control in the previous section is based on the reactor dynamics (1)–(3) and the given—rather heuristical—empirical relations for the reaction heat Q_{rea} and the overall heat transfer coefficient U in Table 2. Therefore, with respect to a general process control which allows the production of multiple products, it is desirable to calculate the feedforward control online. However, this requires the estimation of the time-dependent quantities $Q_{\mathrm{rea}}(t)$ and $U(t)$ during the successive batches.

Fig. 7 shows the block diagram of the considered adaptive feedforward control scheme with an extended Kalman filter (EKF) Σ_{EKF} which uses the available temperature measurements to estimate the reaction heat $\widehat{Q}_{\mathrm{rea}}(t)$ and the heat transfer coefficient $\widehat{U}(t)$. These estimates are used in the online design of the feedforward control Σ_{FF}. The design of the extended Kalman filter Σ_{EKF} and the feedforward control Σ_{FF} are explained in the following sections.

4.1. Parameter estimation by extended Kalman filter

An online estimation of the time-dependent reaction heat $Q_{\mathrm{rea}}(t)$ and overall heat transfer coefficient $U(t)$ with an EKF requires a simplified reactor model, which is still accurate enough to obtain reliable estimations. In [7], the detailed reactor model (1)–(5) is approximated by describing the time-delayed inlet and outlet temperatures $T_j^{\mathrm{in}}(t-\theta_1)$ and $T_j^{\mathrm{out}}(t-\theta_2)$ of the cooling jacket by first-order lag elements. However, this leads to an extension of the reference model by two further ODEs.

In this contribution, the reactor model is reduced by omitting the energy balance (5) for the recirculation loop. This is motivated by the fact that the reaction heat $Q_{\mathrm{rea}}(t)$

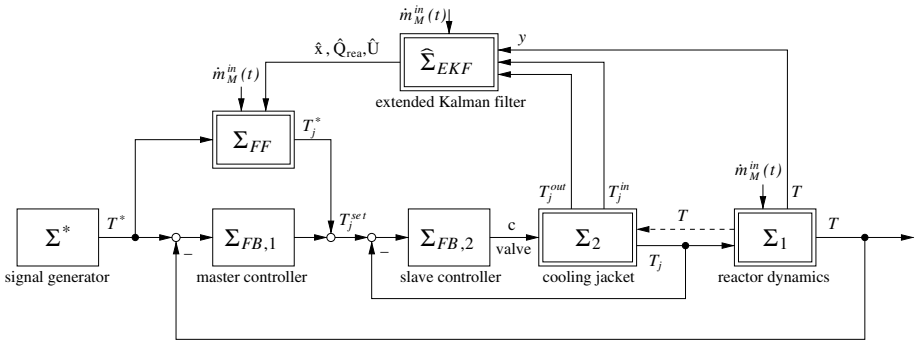

Fig. 7. Control scheme with reactor dynamics Σ_1: (1)–(3), cooling jacket Σ_2: (4) and (5), cascade control $\Sigma_{FB,1}$ and $\Sigma_{FB,2}$ (Section 2.3), adaptive feedforward control Σ_{FF} (Sections 3, and 4.2), and extended Kalman filter $\widehat{\Sigma}_{EKF}$ (Section 4.1).

and the overall heat transfer coefficient $U(t)$ only occur in the energy balances (3) and (4) of the reactor and the cooling jacket. To compensate for the negligence of the ODE (5), the instantaneous and the time-delayed measurements of the inlet temperature $T_j^{in}(t)$ are used in the EKF as known variables

$$\eta_1(t) = T_j^{in}(t), \quad \eta_2(t) = T_j^{in}(t-\theta_1). \tag{15}$$

These variables are inserted in the simplified reactor model

$$\frac{dm_M}{dt} = \dot{m}_M^{in}(t) + \frac{Q_{rea}}{\Delta H}, \tag{16}$$

$$\frac{dm_P}{dt} = -\frac{Q_{rea}}{\Delta H}, \tag{17}$$

$$\frac{dT}{dt} = \frac{1}{\sum_i m_i C_{p,i}}\left[\dot{m}_M^{in}(t) C_{p,M}(T_{amb} - T) + Q_{rea} - UA(T - \overline{T}_j) - (UA)_{loss}(T - T_{amb})\right], \quad i = M, P, W, \tag{18}$$

$$\frac{dT_j^{out}}{dt} = \frac{1}{m_C C_{p,C}}\left[\dot{m}_C C_{p,C}(\eta_2 - T_j^{out}) + UA(T - \overline{T}_j)\right] \tag{19}$$

with the mean jacket temperature

$$\overline{T}_j = \frac{T_j^{out} + \eta_1}{2}. \tag{20}$$

The simplified model (15)–(20) is used for the design of the EKF with the measurement vector

$$y_{EKF} = [T, T_j^{out}]^T. \tag{21}$$

Furthermore, model equations are required for the estimation of $Q_{rea}(t)$ and $U(t)$. The simultaneous estimation of the reaction heat and the heat transfer coefficient is a challenging problem due to the highly nonlinear dynamics of the reactor. The gray profiles (- -) in Figs. 8 and 9 show nominal values of $Q_{rea}(t)$ and $U(t)$ for both polymers A and B calculated with the reference reactor model (1)–(5). The reaction heat shows sharp flanks at the beginning and especially at the end of the reaction when the monomer feed $\dot{m}_M^{in}(t)$ stops. Furthermore, the heat transfer coefficient

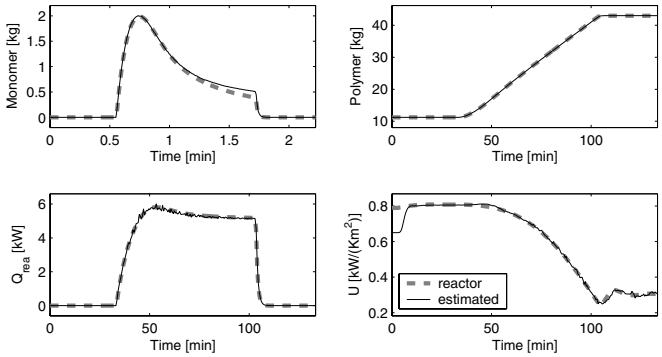

Fig. 8. Simulation results for polymer A: Kalman filter estimates of the reactor with PI cascade control for batch 1 for nominal parameters and summer season.

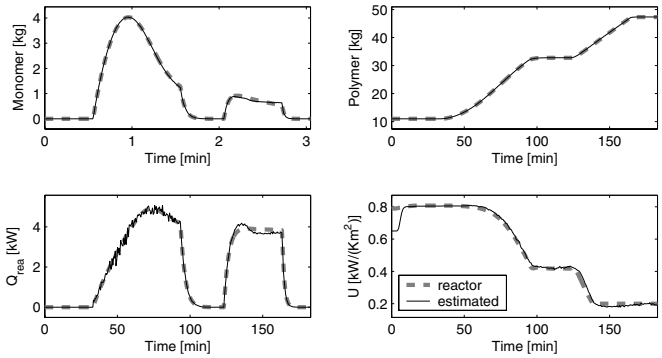

Fig. 9. Simulation results for polymer B: Kalman filter estimates of the reactor with PI cascade control for batch 1 for nominal parameters and summer season.

$U(t)$ decreases significantly during the production and successive batches as viscosity at the wall increases.

In [7], the reaction heat and the heat transfer coefficient are described by a random-walk approach with $\dot{Q}_{rea} = 0$ and $\dot{U} = 0$. However, simulation studies show that the falling flanks of $Q_{rea}(t)$ at $t = t_{M,1}^{in}$ (and $t = t_{M,3}^{in}$ for polymer B) when the monomer feed stops can only be detected with a delay of 50 s or more, even if much system noise is added to

$\dot{Q}_{\mathrm{rea}} = 0$. This delay is too long for using this estimation for a feedforward control design. Similarly, the random-walk approach $\dot{U} = 0$ for the heat transfer coefficient allows to estimate the decrease of $U(t)$ during the production only in a time-delayed manner. A further estimation approach for the Chylla–Haase reactor in [4] uses empirical relations to adequately estimate $Q_{\mathrm{rea}}(t)$ and $U(t)$, e.g., the viscosity is described by an exponential model. However, these empirical relations require process knowledge of every polymer and have to be adopted accordingly.

Therefore, an attempt is made to model the reaction heat $Q_{\mathrm{rea}}(t)$ and the heat transfer coefficient $U(t)$ without using detailed process knowledge, in order to be universally applicable to various products. The reaction heat is modeled by physically reasoning that the reaction heat

$$Q_{\mathrm{rea}}(t) = q_0 m_{\mathrm{M}}(t) \tag{22}$$

is related to the monomer mass $m_{\mathrm{M}}(t)$ with a factor q_0, which has to be estimated instead of directly estimating $Q_{\mathrm{rea}}(t)$. This relation couples the reaction heat $Q_{\mathrm{rea}}(t)$ to the monomer feed $\dot{m}_{\mathrm{M}}^{\mathrm{in}}(t)$ via the material balance (16). This has the advantage that the sharp fall of the reaction heat at the time instant when the monomer feed $\dot{m}_{\mathrm{M}}^{\mathrm{in}}(t)$ stops can be detected without any time delay.

The heat transfer coefficient $U(t)$ is modeled by reasoning that $U(t)$ decreases during the process due to the increase of viscosity at the reactor wall, which again is related to the increasing polymer mass $m_{\mathrm{P}}(t)$. Therefore, the relation

$$U(t) = U_0 + q_1(m_{\mathrm{P}}(t) - m_{\mathrm{P},0}) \tag{23}$$

is assumed, where U_0 is the heat transfer coefficient before the production starts. The second term $q_1(m_{\mathrm{P}} - m_{\mathrm{P},0})$ accounts for the decrease of $U(t)$ during the production with the simultaneous increase of produced polymer $m_{\mathrm{P}}(t)$.[6]

In view of (22) and (23), the EKF model is augmented by the ODEs

$$\dot{q}_0 = 0, \quad \dot{U}_0 = 0, \quad \dot{q}_1 = 0 \tag{24}$$

for the parameters q_0, U_0, and q_1. This yields the overall estimation vector

$$\hat{\boldsymbol{x}} = [\widehat{m}_{\mathrm{M}}, \widehat{m}_{\mathrm{P}}, \widehat{T}, \widehat{T}_j^{\mathrm{out}}, \widehat{q}_0, \widehat{U}_0, \widehat{q}_1]^{\mathrm{T}} \tag{25}$$

with the initial condition

$$\hat{\boldsymbol{x}}(0) = [m_{\mathrm{M},0}, m_{\mathrm{P},0}, T_{\mathrm{amb}}, T_{\mathrm{amb}}, \widehat{q}_0(0), 0, \widehat{U}_0(0), 0]^{\mathrm{T}}, \tag{26}$$

[6] Similar relations for the estimation of $Q_{\mathrm{rea}}(t)$ and $U(t)$ are considered in [5], where a semi-batch process is controlled using model predictive control (MPC). The heat transfer coefficient is modeled as $U(t) = U_0 + \Delta U(t)$, i.e., by estimating $\Delta U(t)$ instead of relating the decay of $U(t)$ to the polymer mass $m_{\mathrm{P}}(t)$ as in (23). Furthermore, the EKF estimates $Q_{\mathrm{rea}}(t)$ with a random-walk approach, whereas the MPC employs a relation similar to (22).

Table 3
Diagonal elements of the system noise covariance matrix

Element	Unit	Heat-up period	1. Feed period	Hold period
$\sigma^2(\widehat{m}_{\mathrm{M}})$	kg^2	0	0	0
$\sigma^2(\widehat{m}_{\mathrm{P}})$	kg^2	0	0	0
$\sigma^2(\widehat{T})$	K^2	0	0	0
$\sigma^2(\widehat{T}_j^{\mathrm{out}})$	K^2	5×10^{-3}	5×10^{-4}	5×10^{-3}
$\sigma^2(\widehat{q}_0)$	$\frac{\mathrm{kW}^2}{\mathrm{kg}^2}$	5×10^{-3}	5×10^{-3}	5×10^{-3}
$\sigma^2(\widehat{U}_0)$	$\frac{\mathrm{kW}^2}{\mathrm{m}^4\,\mathrm{K}^2}$	5×10^{-8}	0	0
$\sigma^2(\widehat{q}_1)$	$\frac{\mathrm{kW}^2}{\mathrm{m}^4\,\mathrm{K}^2\,\mathrm{kg}^2}$	0	5×10^{-8}	5×10^{-9}

see Table A.1. The initial values $\hat{q}_0(0)$ and $\widehat{U}(0)$ are determined by the respective values of the previous batch at the time instant when the monomer starts.

The uncertainties of the system are modeled as system noise in the covariance matrix of the EKF with the respective diagonal elements listed in Table 3. The case-dependent choice of $\sigma^2(\widehat{U}_0)$ and $\sigma^2(\widehat{q})$ is used to estimate $\widehat{U}_0(t)$ during the heat-up before the polymerization starts, and afterwards to estimate $\widehat{q}_1(t)$, respectively. System noise is added to the energy balance (19) of the cooling jacket, i.e., $\sigma^2(\widehat{T}_j^{\mathrm{out}})$, to account for the uncertainties in the delay time θ_1. Furthermore, the value of $\sigma^2(\widehat{q}_1)$ is larger during the monomer feed interval due to the significant decrease of the heat transfer coefficient $\widehat{U}(t)$ via $\widehat{q}_1(t)$ in (23). At the same time the value of $\sigma^2(\widehat{T}_j^{\mathrm{out}})$ is lowered in order to increase the accuracy of the energy balance (19). For the second feed and hold period of polymer B, the parameter settings of the first hold period are used and remain constant.[7]

The covariance matrix of the measurement noise is set to $\mathrm{diag}(\sigma^2(\boldsymbol{y}), \sigma^2(\boldsymbol{y}))$, with the measurement noise $\sigma(\boldsymbol{y}) = 0.05\,\mathrm{K}$ as outlined in Section 2.2. Note that both the reduced measurement vector $\boldsymbol{y}_{\mathrm{EKF}}$ in (21) as well as the auxiliary variables (15) are affected by the measurement noise $\sigma(\boldsymbol{y})$. The sampling time of the EKF is set to 4 s. A smaller sampling time (e.g., 2 s) only slightly increases the estimation performance, whereas sampling times >4 s lead to worse estimation results. Furthermore, the period 4 s is chosen in order to synchronize the EKF with the PI cascade control.

Figs. 8 and 9 show the estimated profiles of $\widehat{m}_{\mathrm{M}}(t)$, $\widehat{m}_{\mathrm{P}}(t)$, $\widehat{Q}_{\mathrm{rea}}(t)$, and $\widehat{U}(t)$ for the polymers A and B compared to the nominal values (- -). For both polymers, the EKF achieves good estimates of $Q_{\mathrm{rea}}(t)$ and $U(t)$. Especially the sharp flanks of the reaction heat $Q_{\mathrm{rea}}(t)$ at the beginning and the end of the monomer feed are detected without any time delay, which is essential in order to use the EKF for an adaptive feedforward control design.

[7] For the sake of simplicity, no cross correlations are considered in the covariance matrix of the system noise, which would form additional degrees-of-freedom to tune the EKF.

4.2. Online feedforward control design

As described in Section 3, the feedforward control $T_j^*(t)$ is determined with the inverse energy balance (3)

$$T_j^* = T^* + \frac{1}{U^* A^*}\left[\sum_i m_i^* C_{p,i}\cdot \dot{T}^* - \dot{m}_{\mathrm{M}}^{\mathrm{in}}(t) C_{p,\mathrm{M}}(T_{\mathrm{amb}} - T^*). \right.$$
$$\left. -Q_{\mathrm{rea}} + (UA)_{\mathrm{loss}}(T^*(t) - T_{\mathrm{amb}})\right]$$
$$= \tilde{\alpha}^{-1}(\dot{m}_{\mathrm{M}}^{\mathrm{in}}(t), m_{\mathrm{M}}^*, m_{\mathrm{P}}^*, Q_{\mathrm{rea}}^*, U^*, T^*, \dot{T}^*) \quad (27)$$

that depends on the desired reactor temperature $T^*(t) \in \mathscr{C}^1$ and the trajectories $m_{\mathrm{M}}^*(t)$, $m_{\mathrm{P}}^*(t)$, $Q_{\mathrm{rea}}^*(t)$, $U^*(t)$. Thereby, the calculation of the reaction heat coefficient $Q_{\mathrm{rea}}^*(t)$ and the heat transfer coefficient $U^*(t)$ is now based on the estimations of the EKF, instead of using the empirical relations in Table 2.

The adaptive design calculates the feedforward control (27) in each time instant t_k over the next time interval $t \in [t_k, t_{k+1}]$. Thereby, the interval length $t_{k+1} - t_k = \Delta t_{\mathrm{FF}}$ is given by the feedforward sampling time Δt_{FF}. Similar to the offline design in Section 3, the trajectories $m_{\mathrm{M}}^*(t)$, $m_{\mathrm{P}}^*(t)$ are calculated over the time interval $t \in [t_k, t_{k+1}]$ by integrating the internal dynamics, i.e., the material balances (1) and (2) with the relation (22):

$$\dot{m}_{\mathrm{M}}^* = \dot{m}_{\mathrm{M}}^{\mathrm{in}}(t) + \frac{\widehat{q}_0(t_k) m_{\mathrm{M}}^*}{\Delta H}, \quad m_{\mathrm{M}}^*(t_k) = \widehat{m}_{\mathrm{M}}(t_k), \quad (28)$$

$$\dot{m}_{\mathrm{P}}^* = -\frac{\widehat{q}_0(t_k) m_{\mathrm{M}}^*}{\Delta H}, \quad m_{\mathrm{P}}^*(t_k) = \widehat{m}_{\mathrm{P}}(t_k). \quad (29)$$

The initial values $\widehat{m}_{\mathrm{M}}(t_k)$, $\widehat{m}_{\mathrm{P}}(t_k)$, and $\widehat{q}_0(t_k)$ are provided by the Kalman filter at time instant t_k.

With the trajectories $m_{\mathrm{M}}^*(t)$ and $m_{\mathrm{P}}^*(t)$, the reaction heat and the heat transfer coefficient are given by

$$Q_{\mathrm{rea}}^*(t) = \widehat{q}_0(t_k) m_{\mathrm{M}}^*(t), \quad (30)$$

$$U^*(t) = \widehat{U}_0(t_k) + \widehat{q}_1(t_k)(m_{\mathrm{P}}^*(t) - m_{\mathrm{P},0}), \quad t \in [t_k, t_{k+1}]. \quad (31)$$

Placing $m_{\mathrm{M}}^*(t)$, $m_{\mathrm{P}}^*(r)$, and (30), (31) in (27) finally yields the feedforward control $T_j^*(t)$ for the time interval $t \in [t_k, t_{k+1}]$, which is used for the setpoint (10) of the slave controller. The sampling time for the adaptive feedforward control is chosen to 4 s in order to synchronize the overall control scheme.[8] Worth noting is that the reactor temperature $T^*(t)$ in (27) is given by the desired trajectory (9) instead of using the actual measured temperature $T(t)$. This ensures the feedforward idea of the concept.

5. Evaluation of the adaptive feedforward/feedback control scheme

The adaptive feedforward control scheme is analyzed in simulation studies under the disturbances as outlined in [2]. Furthermore, a robustness analysis is carried out in order to compare the performance and robustness with respect to the conventional PI cascade control structure.

5.1. Simulation results

The simulation results for both polymers A and B with nominal parameter values are depicted in Figs. 10 and 11. The adaptive feedforward control $T_j^*(t)$ achieves a good approximation compared to the nominal case calculated with (14), see Fig. 12. Especially at the critical time points $t = t_{\mathrm{M},1}^{\mathrm{in}}$ and $t = t_{\mathrm{M},3}^{\mathrm{in}}$ when the monomer feed stops, the feedforward control $T_j^*(t)$ sharply increases without any time delay to the nominal case. This is mainly due to relation (22) of the EKF, which enables the fast detection of the sharp flank of the reaction heat Q_{rea} at the end of the monomer feed.

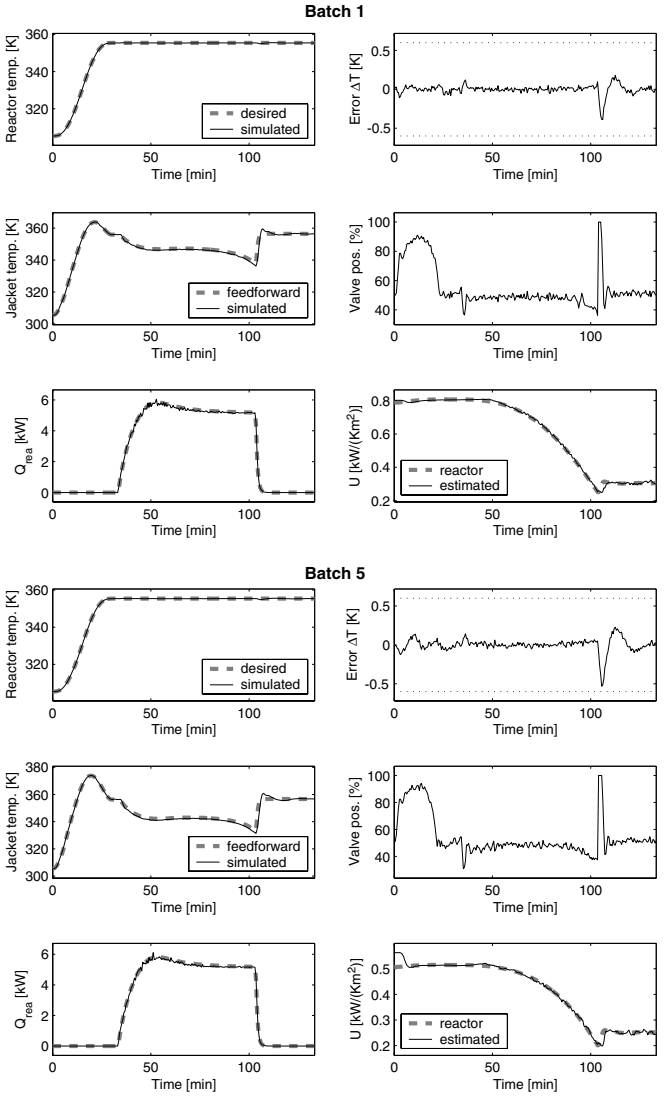

Fig. 10. Simulation results for polymer A, batch no. 1 and 5: adaptive feedforward control with PI cascade control for nominal parameters and summer season.

[8] The sampling time for the feedforward control could by considerably larger than 4 s since it does not directly influence the stability of the overall system. In contrast to this, increasing the sampling time of the underlying cascade feedback control would lead to a worse control performance.

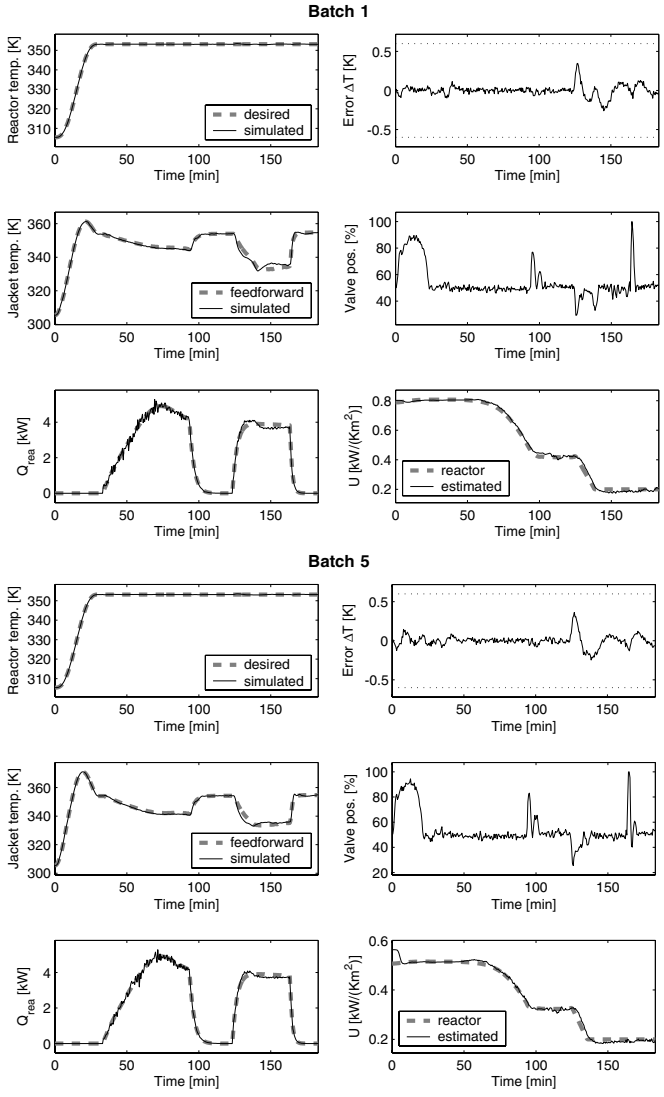

Fig. 11. Simulation results for polymer *B*, batch no. 1 and 5: adaptive feedforward control with PI cascade control for nominal parameters and summer season.

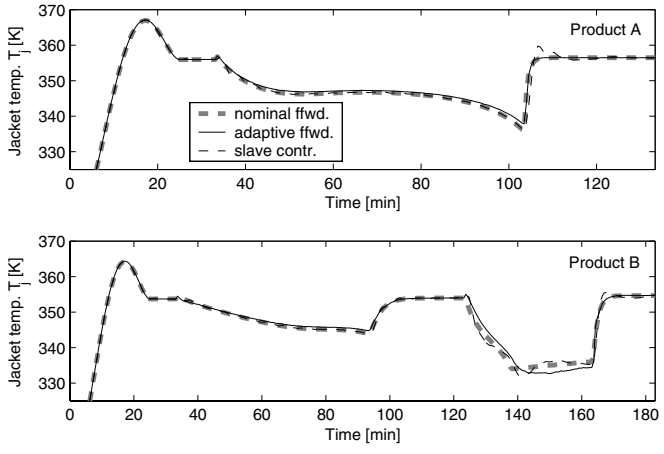

Fig. 12. Simulation results for polymer *A* and *B*: comparison of the offline calculated (nominal) and adaptive feedforward trajectories $T_j^*(t)$, and the controlled jacket temperature $T_j(t)$ for nominal parameters and summer season.

The robustness of the adaptive control scheme is illustrated for a worst case scenario with a +25% mismatch in both delay times θ_1 and θ_2 of the cooling jacket and recirculation loop, as well as a +20% increase of the polymerization rate (i.e., $i = 1.2$ in Table 2). Furthermore, it is assumed that the reactor is operated in the winter season, where the low ambient temperature T_{amb} (see Table A.2) poses higher demands on the cascade control during the heat-up of the reactor. Figs. 13 and 14 show the good performance and robustness of the adaptive control scheme, particularly in combination with the conventional PI cascade control. The EKF provides robust estimates of the reaction heat $Q_{\text{rea}}(t)$ and the heat transfer coefficient $U(t)$, and the reactor temperature $T(t)$ stays within the specified tolerance interval of ± 0.6 K.

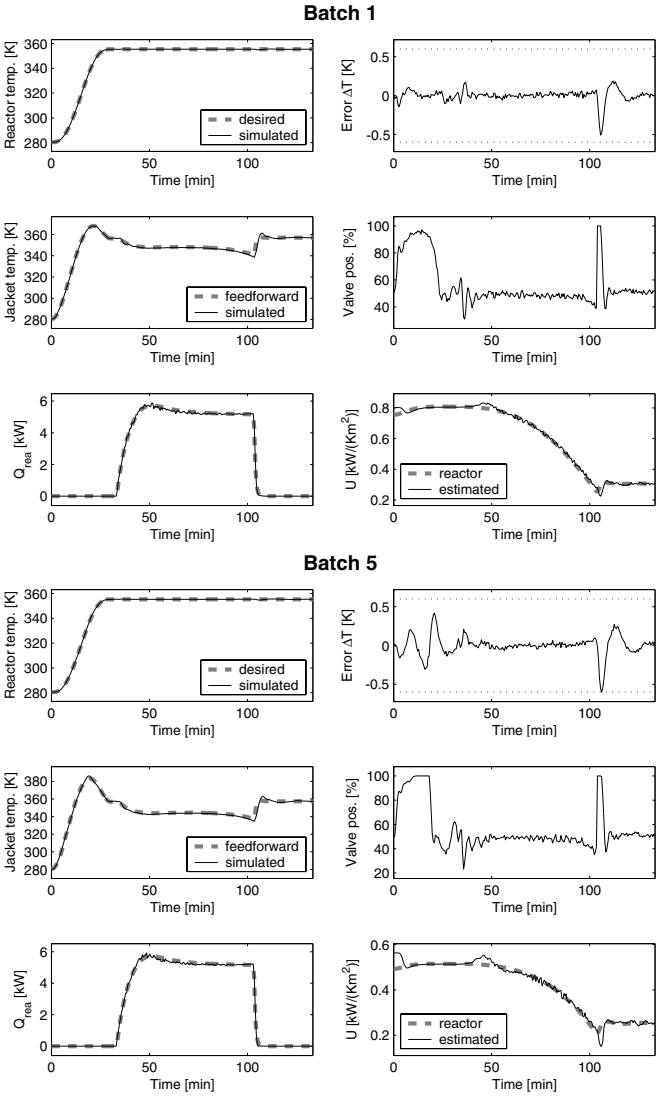

Fig. 13. Simulation results for polymer *A*, batch no. 1 and 5: adaptive feedforward control with PI cascade control for delay times θ_1, $\theta_2 + 25\%$, +20% higher rate of polymerization, and winter season.

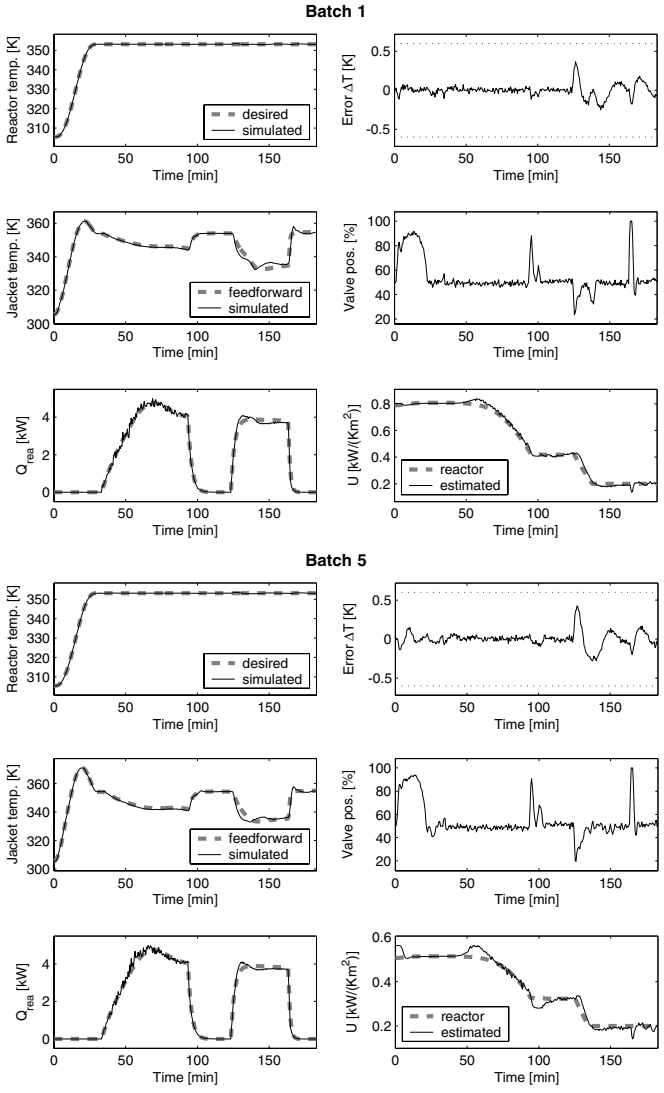

Fig. 14. Simulation results for polymer *B*, batch no. 1 and 5: adaptive feedforward control with PI cascade control for delay times θ_1, $\theta_2 + 25\%$, +20% higher rate of polymerization, and winter season.

5.2. Robustness analysis

The performance of the adaptive feedforward control scheme is compared to the conventional PI cascade control with respect to model uncertainties and measurement errors. The basis for the simulation studies forms the fifth batch for the production of polymer *A*, since it poses the highest demands on the control structure. Thereby, several criteria are used to evaluate the controller performance, see Table 4. The maximum absolute value of the temperature error $\Delta T = \Delta T(t) - T^{\text{set}}$ rates the overall control performance during production. The mean absolute values of the estimation errors $\Delta Q_{\text{rea}} = \widehat{Q}_{\text{rea}} - Q_{\text{rea}}$ and $\Delta U = \widehat{U} - U$ are used as a measure for the estimation performance of the EKF. The mean absolute value of the master controller correction ΔT_j in (10) is a measure for the accuracy of the feedforward control T_j^*. Finally, the standard deviation $\sigma(c)$ of the valve c captures the activity of the slave controller to maintain the reactor temperature $T(t)$ in the tolerance interval ± 0.6 K.

The first two scenarios (i) and (ii) in Table 4 summarize the results for the nominal case and the worst scenario which are already depicted in Figs. 10 and 13. The third scenario (iii) shows an increase of the measurement noise to $\sigma(\boldsymbol{y}) = 0.1$ K, which leads to a larger estimation error of the reaction heat Q_{rea} and a higher activity of the valve c as the manipulated variable of the slave controller. Thereby, $\sigma(c)$ denotes the standard deviation of the valve c during the monomer feed interval as a measure for the valve action. Thereby, $\sigma(c)$ is generally higher for the adaptive feedforward control scheme compared to the conventional cascade control, since the Kalman estimates of $\widehat{Q}_{\text{rea}}$ and $\widehat{U}$ still contain some noise and are used to adapt the feedforward control (27).

In scenario (iv), the monomer feed rate $\dot{m}_{\text{M}}^{\text{in}}(t)$ is increased by 10% (i.e., $1.1 \times \dot{m}_{\text{M}}^{\text{in,max}}$ in (8)), which corresponds to a model mismatch in the energy balance (18) of the EKF and in the feedforward control (27). As a result, the mean estimation error of the reaction heat Q_{rea} increases significantly. This also falsifies the feedforward control $T_j^*(t)$, which the feedback part ΔT_j in (10) has to correct. This scenario clearly shows that an accurate model is necessary for the design of the feedforward control and the EKF. Nevertheless, the combined feedforward/feedback control scheme still achieves a higher control performance compared to the conventional cascade control. The increase of the monomer feed $\dot{m}_{\text{M}}^{\text{in}}(t)$ furthermore has the

Table 4
Robustness analysis of the adaptive feedforward control with PI cascade control under various scenarios for polymer *A*, batch 5 (in brackets: conventional PI cascade control)

Criteria	Units	Scenario (i)	Scenario (ii)	(iii) = (ii) and meas. noise $\sigma(\boldsymbol{y}) = 0.1$ K	(iv) = (ii) and feed $\dot{m}_{\text{M}}^{\text{in}}(t) + 10\%$	(v) = (ii) and meas. delay 10 s
Max. temp. error $\lvert\Delta T\rvert$	K	0.5 (1.8)	0.6 (1.8)	0.6 (1.8)	1.0 (2.2)	0.5 (1.8)
Mean estim. error $\lvert\Delta Q_{\text{rea}}\rvert$	kW	0.07 (–)	0.08 (–)	0.08 (–)	0.38 (–)	0.08 (–)
Mean estim. error $\lvert\Delta U\rvert$	kW m^{-2} K^{-1}	0.008 (–)	0.013 (–)	0.016 (–)	0.019 (–)	0.018 (–)
Mean contr. corr. $\lvert\Delta T_j\rvert$	K	1.0 (–)	1.1 (–)	1.2 (–)	2.1 (–)	1.1 (–)
Valve noise $\sigma(c)$	%	2.0 (1.4)	2.0 (1.4)	2.5 (2.3)	2.1 (1.4)	4.0 (2.4)

Scenario (i): nominal parameters, meas. noise $\sigma(\boldsymbol{y}) = 0.05$ K, summer season.
Scenario (ii): delay times θ_1, $\theta_2 + 25\%$, polymerization rate $R_p + 20\%$, meas. noise $\sigma(\boldsymbol{y}) = 0.05$ K, winter season.

effect that the reaction heat Q_{rea} is increased which makes it harder to keep the temperature $T(t)$ within the specified tolerance interval ± 0.6 K.

In the fifth scenario (v) in Table 4, an additional delay time is considered for the temperature measurements (6) of the reactor and the cooling jacket. The time delay is increased to 10 s until the slave controller starts oscillating (leading to an increased valve action $\sigma(c)$) but still provides a stable operation. The adaptive feedforward control scheme still outperforms the conventional cascade structure, but the significantly higher valve action $\sigma(c)$ reveals that the oscillations of the valve c and of the reactor states are increased by the feedforward control due to the feedback connection with the EKF. This shows that a stable operation of the cascade control and of the EKF must be guaranteed in order to not influence the stability of the overall system by the adaptive feedforward control.

6. Conclusions

The extension of the conventional cascade control by an adaptive feedforward control is studied for the polymerization reactor benchmark problem defined by Chylla and Haase. The resulting two-degree-of-freedom control scheme maintains the structure of the cascade control, which is of importance for industrial applications. The online adaptation of the feedforward control by an extended Kalman filter requires an accurate estimation of the heat transfer coefficient and especially of the reaction heat. The fast detection of the falling flank at the end of the reaction is crucial for the performance of the feedforward control. Therefore, physically motivated relations for the heat transfer coefficient and reaction heat account are derived, which provide an accurate estimate. Especially the reaction heat is estimated without any time delay. These relations are not based on exact process knowledge and are therefore applicable to a wider range of batch reactors. Currently, these relations for estimating the reaction heat and heat transfer coefficient are in the process of being implemented in the distributed control system (DCS) at *BASF Aktiengesellschaft*, Ludwigshafen (Germany) for an advanced process control application.

Acknowledgements

The authors gratefully acknowledge the constructive comments of the reviewers as well as the helpful discussions with Marcus Nohr of *BASF Aktiengesellschaft*, Ludwigshafen (Germany).

Appendix A. Parameters of the Chylla–Haase reactor

Tables A.1 and A.2.

Table A.1
Data of polymers A and B [2,8]

Symbol	Units	Value for A	Value for B
$m_{M,0}$	kg	0.0	0.0
$m_{P,0}$	kg	53.98	42.32
m_W	kg	205.50	165.13
ρ_M	kg m^{-3}	900.0	900.0
ρ_P	kg m^{-3}	1040.0	1040.0
ρ_W	kg m^{-3}	1000.0	1000.0
$C_{p,M}$	kJ kg^{-1} K^{-1}	1.675	1.675
$C_{p,P}$	kJ kg^{-1} K^{-1}	3.140	3.140
$C_{p,W}$	kJ kg^{-1} K^{-1}	4.187	4.187
MW_M	kg kmol^{-1}	104.0	106.0
m_C	kg	42.750	42.996
$\dot{m}_C$	kg/s	0.9412	0.9412
$C_{p,C}$	kJ kg^{-1} K^{-1}	4.187	4.187
k_0	s^{-1}	55	20
k_1	m s kg^{-1}	1000	1000
k_2	–	0.4	0.4
E	kJ kmol^{-1}	29,560.89	29,560.89
c_0	kg m^{-1} s^{-1}	5.2×10^{-5}	3.2×10^{-5}
c_1	–	16.4	19.1
c_2	–	2.3	2.3
c_3	–	1.563	1.563
a_0	K	555.556	555.556
$-\Delta H_p$	kJ kmol^{-1}	−70,152.16	−65593.2
d_0	kW m^{-2} K^{-1}	0.814	0.814
d_1	m s kg^{-1}	−5.13	−5.13
$\dot{m}_M^{in,max}$	kg/s	7.560×10^{-3}	6.048×10^{-3}
$[t_{M,0}^{in}, t_{M,1}^{in}]$	min	[30, 100]	[30, 90]
$[t_{M,2}^{in}, t_{M,3}^{in}]$	min		[120, 160]
T^{set}	K	355.382	353.160

Table A.2
Data of reactor parameters [2,8]

Symbol	Units	Value
R	kJ kmol^{-1} K^{-1}	8.314
$(UA)_{loss}$	kW K^{-1}	0.00567567
τ_p	s	40.2
θ_1	s	22.8
θ_2	s	15.0
i	–	[0.8, 1.2]
$1/h_f$	m^2 K kW^{-1}	[0.000, 0.176, 0.352, 0.528, 0.704]
T_{amb}	K	280.382 (winter), 305.382 (summer)
T_{inlet}	K	294.26
T_{steam}	K	449.82

References

[1] A. Bhat, R.N. Banavar, The Chylla–Haase-problem: a neural network controller, in: Proc. IEEE Int. Conf. Contr. Appl. (CCA), Trieste, Italy, September 1998, pp. 192–196.
[2] R.W. Chylla, D.R. Haase, Temperature control of semi-batch polymerization reactors, Comput. Chem. Eng. 17 (1993) 257–264.
[3] R.W. Chylla, D.R. Haase, Temperature control of semi-batch polymerization reactors (corrigenda), Comput. Chem. Eng. 17 (1993) 1213.
[4] T. Clarke-Pringle, J.F. MacGregor, Nonlinear adaptive temperature control of multi-product, semi-batch polymerization reactors, Comput. Chem. Eng. 21 (12) (1997) 1395–1409.

[5] A. Cruse, W. Marquardt, A. Helbig, J.-S. Kussi, Optimizing adaptive calorimetric model predictive control of a benchmark semi-batch reaction process, in: Proc. 15th IFAC World Congress, Barcelona, Spain, July 2002.
[6] S. Devasia, D. Chen, B. Paden, Nonlinear inversion-based output tracking, IEEE Trans. Automat. Contr. 41 (1996) 930–942.
[7] A. Helbig, O. Abel, A. M'hamdi, W. Marquardt, Analysis and nonlinear model predictive control of the Chylla–Haase benchmark problem, in: Proc. UKACC Int. Conf. Control, Exeter, England, September 1996, pp. 1172–1177.
[8] H. Hinsberger, S. Miesbach, H.J. Pesch, Optimal temperature control of semibatch polymerization reactors, in: F. Keil, W. Mackens, H. Voß, J. Werther (Eds.), Scientific Computing in Chemical Engineering, Springer, 1996, pp. 75–83.
[9] A. Isidori, Nonlinear Control Systems, third ed., Springer, 1995.